Eur. Phys. J. B **30**, 469–479 (2002)
DOI: 10.1140/epjb/e2002-00403-7

THE EUROPEAN PHYSICAL JOURNAL B

Magnetic properties of $LaNi_{1-x}Mn_xO_{3+\delta}$ perovskites

J. Blasco[1,a], J. García[1], M.C. Sánchez[1], J. Campo[1,2], G. Subías[1,3], and J. Pérez-Cacho[1]

[1] Instituto de Ciencia de Materiales de Aragón and Departamento de Física de la Materia Condensada, Consejo Superior de Investigaciones Científicas y Universidad de Zaragoza, 50009 Zaragoza, Spain
[2] Institut Laue-Langevin, BP 156, 38042 Grenoble Cédex 9, France
[3] ESRF, BP 220, 38043 Grenoble, France

Received 19 July 2002 / Received in final form 23 October 2002
Published online 31 December 2002 –

Abstract. Magnetic measurements have been carried out in different $LaNi_{1-x}Mn_xO_{3+\delta}$ samples with $0.1 \leq x \leq 0.9$. All these samples show two magnetic anomalies, one at relatively high temperature characteristic of a ferromagnetic ordering and the other at low temperature, typical of magnetic relaxation phenomena. Neutron diffraction patterns indicate that long-range ferromagnetic ordering is only achieved for $x \geq 0.5$. Neutron patterns of $LaNi_{0.5}Mn_{0.5}O_{3+\delta}$ samples show an ordered arrangement of Ni and Mn atoms in the perovskite lattice. $LaNi_{0.5}Mn_{0.5}O_{3+\delta}$ is then, a double perovskite $A_2BB'O_6$ whereas Ni and Mn atoms are randomly distributed for the rest of the samples. X-ray magnetic circular dichroism experiments confirm the presence of collinear ferromagnetism in $LaNi_{0.5}Mn_{0.5}O_{3+\delta}$. The role of competitive magnetic interactions, structural disorder, magnetic anisotropy and magnetic disaccommodation is also discussed

PACS. 75.25.+z Spin arrangements in magnetically ordered materials (including neutron and spin-polarized electron studies, synchrotron-source X-ray scattering, etc.) – 75.10.Nr Spin-glass and other random models – 61.12.-q Neutron diffraction and scattering – 75.50.Dd Nonmetallic ferromagnetic materials

1 Introduction

The recent discovery of giant magnetoresistance [1] in mixed oxides of manganese, the so-called manganites, has stimulated the research in related compounds. The $LaNi_{1-x}Mn_xO_3$ series was studied in the past but their magnetic properties are not completely understood so far. Goodenough *et al.* reported that ternary oxides $LaNi_{1-x}Mn_xO_3$ are ferromagnets [2]. The ferromagnetism is observed [3,4] in practically the whole series ($0.1 \leq x \leq 0.9$). The magnetic moment increases as the Mn content increases but the opposite trend is observed for the Curie temperature (T_C). The latter achieves its maximum value [4] for $x = 0.5$ and remains almost constant for $x < 0.5$. This result made several authors [4–7] suggest the presence of phase segregation into $LaMn_{1/2}Ni_{1/2}O_3$ and $LaNiO_3$ for $x < 0.5$ to account for the magnetic properties. Other authors instead [3], claim for a solid solution in the whole composition range.

Blasse suggested the ferromagnetism to be governed by the positive superexchange interaction between Ni^{2+} and Mn^{4+} ions *via* oxygen anions [8] and a partial ordering of Ni^{2+} and Mn^{4+} was proposed to explain the ferromagnetic ground state for $LaNi_{0.5}Mn_{0.5}O_3$. However, several studies performed on this series obtained different conclusions about the electronic state of Ni and Mn atoms in these compounds. Some authors claimed [3,9] for a homovalent substitution between Ni^{3+} and Mn^{3+} whereas other works reported [4–8] the presence of Mn^{4+} and Ni^{2+} ions. Electrical properties were also studied in the past. The $LaNi_{1-x}Mn_xO_3$ samples are semiconducting [3] for $x \geq 0.1$ and the highest activation energy is achieved between $x = 0.5$ and $x = 0.6$ [4].

We have recently performed several works on this series that have thrown light on the structure and electronic properties of this system. Our structural study [10] have shown the existence of solid solution in $LaNi_{1-x}Mn_xO_3$ for any value of x. In particular, transmission electron microscopy [11] confirmed the existence of the $LaNi_{0.75}Mn_{0.25}O_3$ as a single phase. Furthermore, we have determined the local structure and the electronic properties by means of X-ray absorption spectroscopy [12]. This study clearly demonstrates that the more suitable "ionic" approximation to describe the $LaNi_{0.5}Mn_{0.5}O_3$ compound would be $La_2Ni^{2+}Mn^{4+}O_6$. Furthermore, the addition of Ni to $LaMnO_3$ oxidizes the Mn sublattice (Ni being as Ni^{2+}). In the same way, the incorporation of Mn to $LaNiO_3$ leads to reduction of Ni^{3+} (and then, an oxidation from Mn^{3+} to Mn^{4+}).

Bearing in mind these results, we now want to study the magnetic properties of this series by using macroscopic magnetic measurements and neutron diffraction experiments. Here, we report ac magnetic susceptibility, dc magnetization and neutron diffraction measurements on

[a] e-mail: jbc@posta.unizar.es

Table 1. Oxygen content, space group and lattice parameters (Ref. [10] at room temperature. O-sintered refers to samples sintered in oxygen at 900 °C for 2 d. Air-sintered: as above plus a sintering step in air at 1400 °C for 12 h. A-sintered: as air-sintered plus a sintering step in Argon at 1000 °C for 12 h. N-sintered: as air-sintered plus a sintering step in nitrogen at 1400 °C for 12 h. (*) The space groups are taken from reference [10], the present work shows that R $\bar{3}$ and $P2_1/n$ are more appropriate to describe these crystallographic phases. The cationic ratio (La:Mn:Ni) was verified by EDS analysis as indicated in reference [11].

Sample	Oxygen content (δ)	Space group	Lattice parameters (Å)
O-sintered $LaNi_{0.9}Mn_{0.1}O_{3+\delta}$	0.02	R $\bar{3}$ c	$a = 5.461$; $c = 13.165$
O-sintered $LaNi_{0.75}Mn_{0.25}O_{3+\delta}$	0.0	R $\bar{3}$ c	$a = 5.580$; $c = 13.198$
O-sintered $LaNi_{0.5}Mn_{0.5}O_{3+\delta}$	0.08	*R $\bar{3}$ c + Pbnm	$a = 5.504$; $c = 13.237$
		66% + 34%	$a = 5.502$; $b = 5.450$; $c = 7.736$
Air-sintered $LaNi_{0.5}Mn_{0.5}O_{3+\delta}$	0.06	*R $\bar{3}$ c + Pbnm	$a = 5.505$; $c = 13.235$
		42% + 58%	$a = 5.503$; $b = 5.453$; $c = 7.738$
A-sintered $LaNi_{0.5}Mn_{0.5}O_{3+\delta}$	0.05	*R $\bar{3}$ c + Pbnm	$a = 5.513$; $c = 13.236$
		32% + 68%	$a = 5.512$; $b = 5.458$; $c = 7.739$
O-sintered $LaNi_{0.25}Mn_{0.75}O_{3+\delta}$	0.09	Pbnm	$a = 5.520$; $b = 5.471$; $c = 7.756$
Air-sintered $LaNi_{0.25}Mn_{0.75}O_{3+\delta}$	0.05	Pbnm	$a = 5.528$; $b = 5.499$; $c = 7.786$
A-sintered $LaNi_{0.25}Mn_{0.75}O_{3+\delta}$	0.0	Pbnm	$a = 5.532$; $b = 5.498$; $c = 7.788$
N-sintered $LaNi_{0.25}Mn_{0.75}O_{3+\delta}$	−0.03	Pbnm	$a = 5.531$; $b = 5.504$; $c = 7.792$
O-sintered $LaNi_{0.1}Mn_{0.9}O_{3+\delta}$	0.13	R $\bar{3}$ c	$a = 5.521$; $c = 13.327$
Air-sintered $LaNi_{0.1}Mn_{0.9}O_{3+\delta}$	0.06	Pbnm	$a = 5.533$; $b = 5.494$; $c = 7.784$
A-sintered $LaNi_{0.1}Mn_{0.9}O_{3+\delta}$	0.02	Pbnm	$a = 5.531$; $b = 5.555$; $c = 7.801$
N-sintered $LaNi_{0.1}Mn_{0.9}O_{3+\delta}$	−0.02	Pbnm	$a = 5.531$; $b = 5.582$; $c = 7.788$

the $LaNi_{1-x}Mn_xO_3$ samples. In addition, X-ray magnetic circular dichroism (XMCD) has been used to investigate the specific magnetic ordering of Mn and Ni atoms in the $LaNi_{0.5}Mn_{0.5}O_{3.06}$ sample. The XMCD signal is directly related to the local magnetic moment of the photoexcited atom when the core electron is promoted into final states that are responsible for ferro- and ferrimagnetic behaviors.

Neutron diffraction studies available so far concern to the undoped compounds: $LaMnO_3$ and $LaNiO_3$. The latter is paramagnetic [13] down to 1.5 K while the former shows an antiferromagnetic lattice with ferromagnetic coupling of the Mn ions within the plane (001) and antiferromagnetic interactions between planes [14]. However, the magnetism is different for oxidized $LaMnO_{3+\delta}$. The antiferromagnetic order evolves towards a ferromagnetic order as δ increases [15]. This behavior is coupled to a drastic reduction of the static Jahn-Teller distortion of the MnO_6 octahedra. One of the aims of this work includes the study of these features in the $LaNi_{1-x}Mn_xO_3$ series. Moreover, our previous crystallographic and spectroscopic works [10,12] pointed out to partial ordering of Mn^{4+} and Ni^{2+} in $LaNi_{0.5}Mn_{0.5}O_{3+\delta}$ as suggested by Blasse [8]. We have now investigated this point giving an experimental support to that hypothesis.

2 Experimental section

The preparation and characterization of $LaNi_{1-x}Mn_xO_{3+\delta}$ ($x = 0.1$, 0.25, 0.5, 0.75, 0.9) samples have been reported elsewhere [10]. We briefly summarize some details for the sake of clarity. The samples were prepared following a citrate route. Different sintering conditions were used to obtain samples with different degree of oxidation. The sintering conditions and oxygen content of the samples are summarized in Table 1. The samples are denoted as O-sintered, air-sintered, A-sintered and N-sintered according to the sintering conditions (see Tab. 1). The oxygen content of the samples was determined from thermogravimetric analysis in a reducing atmosphere ($Ar/H_2 = 95/5$). It is well known that oxidized samples have cationic vacancies [16] but we use the $LaMnO_{3+\delta}$ nomenclature for the sake of clarity.

All samples were characterized by X-ray powder diffraction at room temperature by using a D-max Rigaku system with a rotating anode and selecting the Cu K_α radiation. The respective lattice parameters and space groups are also shown in Table 1.

Neutron diffraction experiments were performed at the high flux reactor of the ILL (Grenoble). The high flux 2-axis powder diffractometer D1B instrument was used for the thermodiffractometric study. A pyrolytic graphite (002) focusing monochromator, giving a 2.52 Å wavelength, was employed in this experiment. The ^{3}He/Xe position sensitive detector, which covered a 2θ angular range from 20 up to 100 degrees, allowed us to collect spectra each 5 minutes. Patterns were recorded as temperature was slowly increased from 1.5 up to 300 K using a standard orange cryostat.

The $LaNi_{0.5}Mn_{0.5}O_{3.06}$ sample was also studied in the high-resolution diffractometer D1A of ILL working with 1.9114 Å wavelength. The diffractograms were collected at 1.5 and 400 K with 7 h of acquisition time and using a standard orange cryo-oven. Sample containers used in neutron diffraction experiments were vanadium cylinders of 6 mm of diameter.

The crystal structures were refined by the Rietveld method using the Fullprof program [17]. Magnetic measurements were performed between 5 and 400 K in a commercial Quantum Design (SQUID) magnetometer provided with an ac experimental setup. Measurements of magnetic ac susceptibility were carried out at frequencies ranging from 0.12 to 120 Hz and amplitude of the alternating field of 4.5 Oe.

XMCD measurements at Mn and Ni $L_{2,3}$ edges ($2p \rightarrow 3d$ transitions) of the $LaNi_{0.5}Mn_{0.5}O_{3.06}$ sample were performed in total electron yield detection mode on the Dragon beamline (ID8) at ESRF [18]. XMCD signals were obtained as the difference between two X-ray absorption spectra (XAS) recorded consecutively by flipping the applied magnetic field of 4 T parallel and antiparallel to the beam direction for a fixed helicity of the light (right polarization). The measured rate of circular polarization is $P_c = 83(\pm5)\%$ at the Mn $L_{2,3}$ edge and $P_c = 88(\pm5)\%$ at the Ni $L_{2,3}$ edge [19]. All the spectra were recorded after a zero field cooling process down to 50 K, well below the T_C of the sample. The sample was scraped *in situ* before the measurements.

3 Results

3.1 Magnetic measurements

Figures 1 and 2 show the ac susceptibility *vs.* temperature curves of $LaNi_{1-x}Mn_xO_{3+\delta}$. The in-phase, χ', and out-of-phase, χ'', (real and imaginary) components were measured in zero dc field with an alternating field of 4.5 Oe. All of these samples qualitatively show the same behavior. The in-phase component show a sharp increase at relatively high-temperature that can easily be ascribed to a ferromagnetic transition. Then, it shows a complex behavior with decreasing temperature. The χ' component decreases for $x > 0.5$ samples with decreasing temperature with a sharp jump. The samples with $x \leq 0.5$ instead, show a peak below 50 K, better noticed in the χ'' curve (compare Figs. 1 and 2).

The out-of-phase component exhibits two peaks for all samples. The peak observed at the highest temperature corresponds to the T_C. It corresponds with the inflection of the ferromagnetic transition in the χ' curve for samples with $x \geq 0.5$. In the other samples instead ($x = 0.25$ and $x = 0.1$), the maximum of this peak coincides in temperature with the maximum of the χ' curve (compare curves for $x \leq 0.5$ samples in the Fig. 2). The second peak located at low temperature seems to be related to dynamic processes as will be described below.

Table 2 summarizes some magnetic parameters of these samples. We have also observed that T_C increases as the Ni content goes up to $x = 0.5$ in agreement with previous studies [3–7]. The $LaNi_{0.1}Mn_{0.9}O_3$ samples order around 160 K. The exception is the N-sintered sample whose transition is located at 130 K. We note that the more oxidized the sample is, the broader the transition is. The $LaNi_{0.25}Mn_{0.75}O_3$ samples also show a ferromagnetic transition in the range between 200 and 150 K. The

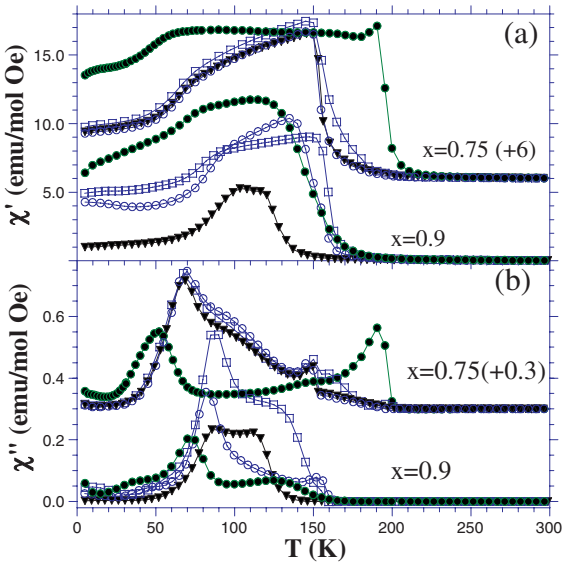

Fig. 1. (a) In-phase and (b) out-of-phase components of the ac magnetic susceptibility for $LaNi_{0.1}Mn_{0.9}O_{3+\delta}$ ($x = 0.9$) and $LaNi_{0.25}Mn_{0.75}O_{3+\delta}$ ($x = 0.75$) samples. Black circles, white circles, squares and triangles refer to O-sintered, air-sintered, A-sintered and N-sintered samples respectively. The $x = 0.75$ samples are shifted upwards (indicated in parenthesis) for the sake of clarity.

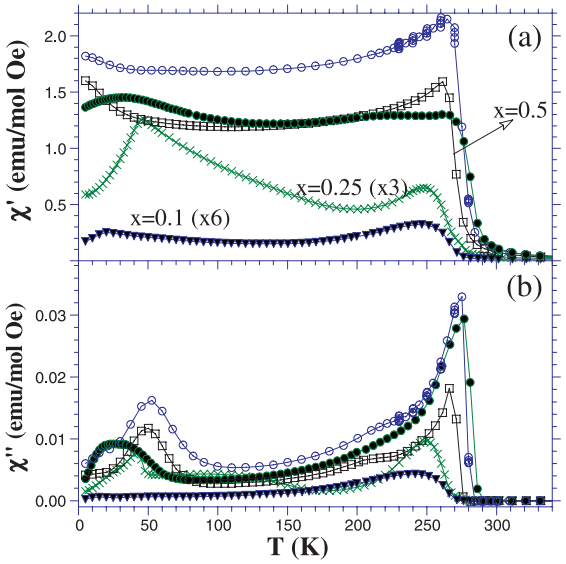

Fig. 2. (a) In-phase and (b) out-of-phase components of the ac magnetic susceptibility for $LaNi_{0.5}Mn_{0.5}O_{3+\delta}$ ($x = 0.5$), $LaNi_{0.75}Mn_{0.25}O_{3.0}$ ($x = 0.25$) and $LaNi_{0.9}Mn_{0.1}O_{3.02}$ ($x = 0.1$) samples. Black circles, white circles and squares refer to O-sintered, air-sintered and A-sintered $LaNi_{0.5}Mn_{0.5}O_3$ samples, respectively. The in-phase data of $x = 0.1$ and $x = 0.25$ samples are multiplied by the factor indicated in parenthesis for the sake of comparison.

Table 2. The Curie temperature, experimental magnetic moment (taken from isothermal magnetization curve at 5 K and from neutron patterns) and theoretical magnetic moment for $LaNi_{1-x}Mn_xO_{3+\delta}$ samples.

Sample	T_C (K)	$M_{(5K,\ 5\ T)}$ (μ_B/fu)	$M_{neut\ 1.5\ K}$ (μ_B/fu)	M_{theor} (μ_B/fu)
$LaNi_{0.9}Mn_{0.1}O_{3.02}$	264	0.13	0	1.3
$LaNi_{0.75}Mn_{0.25}O_{3.0}$	263	0.4	0	2.25
$LaNi_{0.5}Mn_{0.5}O_{3.08}$	280	1.8	1.85(6)	2.34
$LaNi_{0.5}Mn_{0.5}O_{3.06}$	267	1.8	1.80(6)	2.38
$LaNi_{0.5}Mn_{0.5}O_{3.05}$	272	1.85	–	2.4
$LaNi_{0.25}Mn_{0.75}O_{3.09}$	196	2.95	2.37(5)	3.16
$LaNi_{0.25}Mn_{0.75}O_{3.05}$	156	2.98	–	3.2
$LaNi_{0.25}Mn_{0.75}O_{3.0}$	152	3.0	2.76(4)	3.25
$LaNi_{0.25}Mn_{0.75}O_{2.97}$	152	3.15	–	3.26
$LaNi_{0.1}Mn_{0.9}O_{3.13}$	140	3.15	2.40(5)	3.57
$LaNi_{0.1}Mn_{0.9}O_{3.06}$	146	3.6	–	3.64
$LaNi_{0.1}Mn_{0.9}O_{3.02}$	157	3.55	3.32(4)	3.68
$LaNi_{0.1}Mn_{0.9}O_{2.98}$	126	3.6	–	3.71

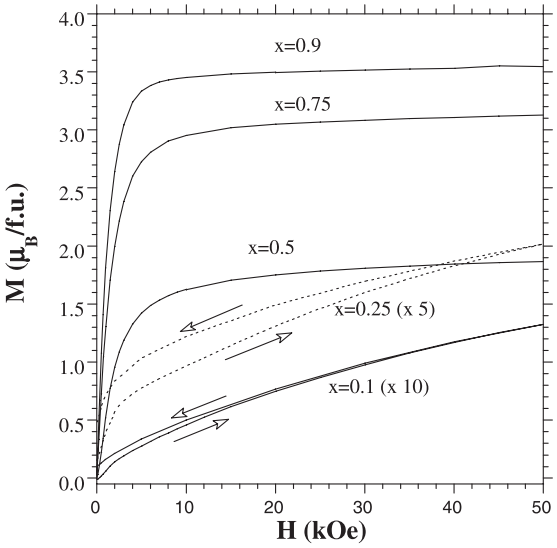

Fig. 3. Isothermal magnetization curves at 5 K for $LaNi_{0.1}Mn_{0.9}O_{3.0}$ ($x = 0.9$), $LaNi_{0.25}Mn_{0.75}O_{3.02}$ ($x = 0.75$), $LaNi_{0.5}Mn_{0.5}O_{3.06}$ ($x = 0.5$), $LaNi_{0.75}Mn_{0.25}O_{3.0}$ ($x = 0.25$) and $LaNi_{0.9}Mn_{0.1}O_{3.02}$ ($x = 0.1$) samples. The data of $x = 0.25$ and $x = 0.1$ samples have been multiplied by 5 and 10, respectively, for the sake of clarity.

highest T_C corresponds to the most oxidized sample. The $LaNi_{0.5}Mn_{0.5}O_3$ samples have the highest T_C in the series (≈265–285 K) whereas the Ni-rich samples ($x < 0.5$) almost have the same T_C (around 260 K).

Another difference among these compounds concerns to the magnitude of the magnetic signal. It decreases as the Mn content does. This is better noticed in Figure 3 where the isothermal *M vs. H* curves at 5 K are plotted for selected compounds. Magnetic saturation is achieved at fields of 1–2 T for $LaNi_{0.1}Mn_{0.9}O_{3.0}$ and $LaNi_{0.25}Mn_{0.75}O_{3.0}$ samples. The saturation values are summarized in Table 2 and they correlate quite well with the theoretical ones considering the spin only contribution of the transition metals. Here we assume $LaNi^{2+}_{1-x}Mn^{4+}_{1-x}Mn^{3+}_{2x-1}O_3$ ($x \geq 0.5$) as a rough ionic approximation (Note that the same magnetic moments are expected for a mixture of only Ni^{3+} and Mn^{3+}). Oxidized samples show the smallest saturation moment (see Tab. 2). This result is related with two effects: a higher transition metal vacancy and high degree of transition-metal oxidation (higher amounts of Mn^{4+} and/or Ni^{3+}). The magnetization curves seem to saturate for the $LaNi_{0.5}Mn_{0.5}O_{3.06}$ sample but saturation is not truly achieved at 5 T because a small positive slope is noticed at high magnetic fields. The lack of magnetic saturation is more evident for $LaNi_{0.75}Mn_{0.25}O_3$ and $LaNi_{0.9}Mn_{0.1}O_3$ samples where a large hysteresis is observed. The experimental and theoretical magnetic moments are compared in Table 2. The experimental values are quite low and they only represent the 75%, 23% and 10% of the magnetic moment expected for $LaNi_{0.5}Mn_{0.5}O_{3.06}$, $LaNi_{0.75}Mn_{0.25}O_3$ and $LaNi_{0.9}Mn_{0.1}O_3$ samples, respectively. In addition, these samples show magnetic anomalies at low temperatures (50 K or below) in the χ' curve that are better noticed in the out-of-phase component (see Fig. 2b). Such kind of anomaly was ascribed to the freezing processes of ferromagnetic clusters in the $LaNi_{0.75}Mn_{0.25}O_3$ compound [11]. These results seem to suggest a lack of magnetic homogeneity in the ground state of $LaNi_{1-x}Mn_xO_{3+\delta}$ samples with $x \leq 0.5$.

We are now focusing again in the $LaNi_{1-x}Mn_xO_{3+\delta}$ samples with $x > 0.5$. These samples show magnetic saturation at 5 K but the magnetic susceptibility shows an anomaly below T_C: The χ' curve decreases as temperature does showing a characteristic inflection point. Accordingly, the χ'' curves show two peaks corresponding to T_C and the mentioned inflection point. Similar features were previously observed in non-stoichiometric $LaMnO_{3+\delta}$ samples [20] and they were ascribed to the presence of randomly oriented ferromagnetic clusters. Actually, the shape

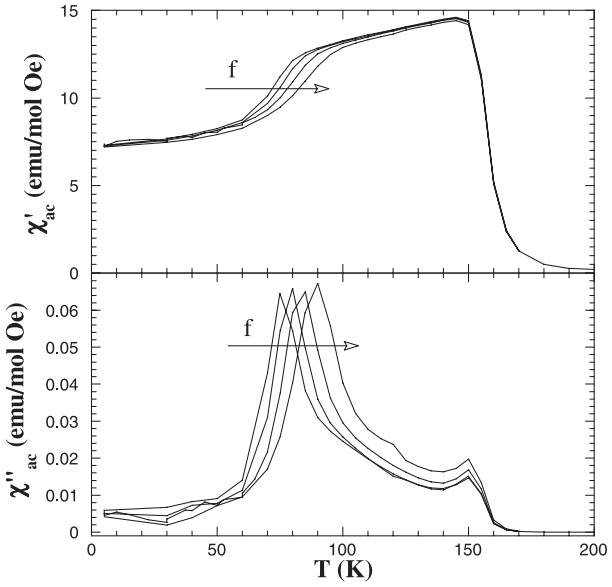

Fig. 4. Ac magnetic susceptibility at different frequencies f of the alternating field (0.2, 1.2, 12 and 120 Hz) for the $LaNi_{0.1}Mn_{0.9}O_{3.02}$ sample. The arrows indicate the frequency increase.

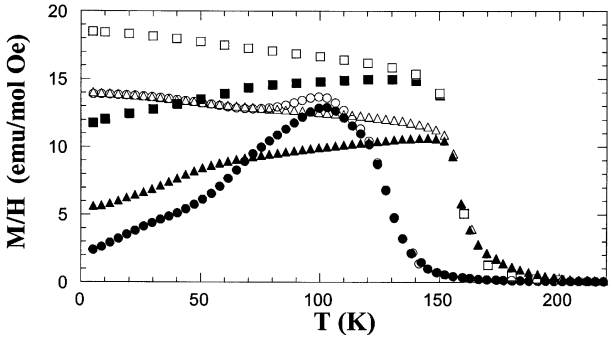

Fig. 5. Thermal dependence of the magnetization for $LaNi_{0.1}Mn_{0.9}O_{2.98}$ (circles), $LaNi_{0.1}Mn_{0.9}O_{3.02}$ (squares), and $LaNi_{0.25}Mn_{0.75}O_{2.97}$ (triangles) samples under an applied field of 1 kOe. The measurements were performed by increasing temperature after cooling the sample in zero-field (black symbols) or under a field of 1 kOe (white symbols).

of the χ' curves can be ascribed to different causes: a spin-glass phase, a reentrant spin-glass system or a change of the magnetic anisotropy in a ferromagnet. In order to characterize it, different magnetic measurements have been performed. Figure 4 shows the ac magnetic susceptibility *vs.* temperature curves, obtained at different frequencies of the alternating field, for $LaNi_{0.1}Mn_{0.9}O_{3.02}$ sample. We observe dynamic behavior in the magnetic susceptibility below T_C. In order to characterize the relaxation phenomena, we have determined the term K, $K = \Delta T_f/[T_f \Delta(\log_{10} f)]$, T_f and f being the freezing temperature of spins (or clusters) and frequency of the alternating field, respectively. Δ refers to difference. We have estimated a value of $K = 6 \times 10^{-2}$, taking the low-temperature peak of χ'' (see Fig. 4) as T_f. This value compares quite well with the value found for typical spin-glass systems [21] such as $(LaGd)Al_2$ or (EuSr)S, and it is practically an order of magnitude lower than the same parameter for a conventional superparamagnet. It is worth pointing out that relaxation phenomena practically begin at T_C. This is better noticed in the χ'' component. The high-temperature χ'' peak ascribed to the ferromagnetic transition also exhibit dynamic behavior. In this case, the amplitude of the peak increases as the frequency does but the position of the peak is almost constant. Similar results were found for the rest of the samples as reported [11] for $LaNi_{3/4}Mn_{1/4}O_3$.

We have also performed dc magnetization measurements registered on warming under an applied dc field of 1 kOe after cooling in this field (FC) or after cooling without field (ZFC). Figure 5 shows several examples of these measurements. ZFC and FC show marked differences at low temperatures for all samples. The ZFC branch shape resembles the ac susceptibility measurements whereas FC branches are characteristic of a conventional ferromagnet. The magnetic irreversibility begins close to T_C, discarding the possibility of a reentrant spin-glass. These features have been ascribed to the lack of a true ferromagnetic ordering transition and the presence instead, of ferromagnetic clusters giving rise to a cluster-glass system. Several examples can be found in the literature such as different doped manganites [22] or cobaltates [23]. However, our neutron diffraction study, reported in the next section, shows the presence of ferromagnetic long-range ordering for $LaNi_{1-x}Mn_xO_{3+\delta}$ samples with $x \geq 0.5$. Therefore, a cluster-glass system does not seem to be suitable to explain the whole magnetic properties of these samples.

3.2 Neutron diffraction

In order to gain insight into the magnetic arrangement of the metal magnetic moments in these compounds, we carried out neutron-diffraction experiments on selected samples: $LaNi_{0.9}Mn_{0.1}O_{3.02}$, $LaNi_{0.75}Mn_{0.25}O_{3.0}$, $LaNi_{0.5}Mn_{0.5}O_{3.06}$, $LaNi_{0.25}Mn_{0.75}O_{3.0}$, $LaNi_{0.25}Mn_{0.75}O_{3.09}$, $LaNi_{0.1}Mn_{0.9}O_{3.02}$, $LaNi_{0.1}Mn_{0.9}O_{3.13}$. The thermal dependence of structural parameters was also studied in a previous work [10]. Summarizing briefly our results, the crystallographic structure of $LaNi_{1-x}Mn_xO_{3+\delta}$ depends on both, the Ni/Mn ratio and the oxygen content. The unit cell of stoichiometric samples ($\delta = 0$) is rhombohedral (space group, R $\bar{3}$ c) for $x < 0.5$ and orthorhombic (space group, Pbnm) for $x > 0.5$. Both phases coexist at room temperature in $LaNi_{0.5}Mn_{0.5}O_3$ (see Tab. 1) because this compound undergoes a structural phase transition just at room temperature. Nevertheless, there are some doubts about the assigned space groups in this case due to the probable ordering of Mn and Ni atoms. Finally, a sample with high Mn content and high value of δ, *i.e.* $LaNi_{0.1}Mn_{0.9}O_{3.13}$, also shows a rhombohedral phase at room temperature that transforms into the orthorhombic phase at around 220 K.

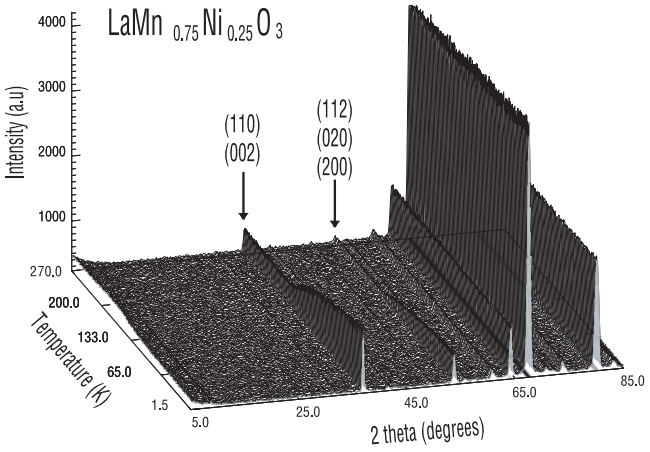

Fig. 6. Neutron thermodiffractograms of $LaNi_{0.25}Mn_{0.75}O_{2.0}$ sample. Arrows indicate the main peaks with ferromagnetic contribution.

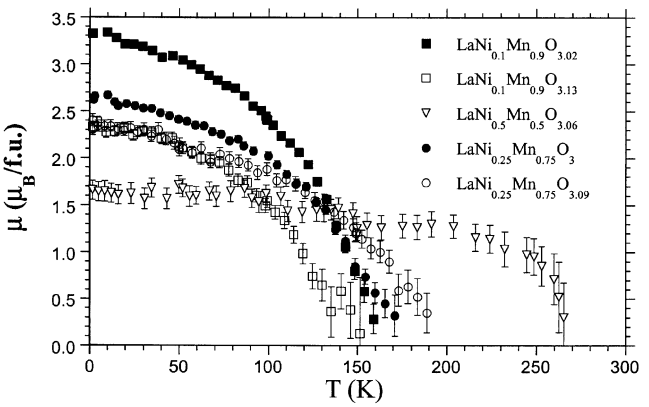

Fig. 7. Magnetic moments of several $x \leq 0.5$ samples indicated in the figure. The data were obtained from the refinement of the neutron patterns. Note: The patterns of the $LaNi_{0.5}Mn_{0.5}O_{3.06}$ sample were refined in the frame of the Pbnm space group as a first approximation.

Regarding the magnetism, different behaviors have been observed in $LaNi_{1-x}Mn_xO_3$ samples depending on the x value. The samples with $x = 0.1$ and 0.25 do not show any remarkable difference between the patterns taken at room temperature and at 1.5 K. The intensities for all reflections remain unchanged, except for the thermal parameter effect. Therefore, any magnetic contribution, if exists, is very small. Either the correlation length is very short or the magnetic fraction is very small. Both samples present the rhombohedral phase in the whole temperature range [10].

The samples with $x \geq 0.5$ (S.G. Pbnm) show a similar behavior. In all of them, as the temperature decreases, a new magnetic scattering contribution appears. This is clearly visible, for example, as an increase of the nuclear reflection (110)+(002) and (112)+(020)+(200). Therefore, the new magnetic phase can be indexed with a propagation vector $K = 0$. For instance, in Figure 6 is displayed the thermodiffractogram in the temperature range from 1.5 to 300 K for the $x = 0.75$ sample. The absence of (001), (111) and (003) AF magnetic reflections located at 2θ values of 18, 42 and 58 degrees, respectively, excludes the presence of AF magnetic order and suggest a magnetic structure where the spins lay in (001) ferromagnetic planes ferromagneticaly coupled along the c axis. The direction in which spins are pointing can not be determined from our data. The thermal variation of the refined magnetic moment for these samples is displayed in Figure 7. The ferromagnetism onset and the values of the ordered moment at low temperature depend on the x value. The T_C increases as the Ni content does whereas the magnetic moment decreases, in agreement with the macroscopic magnetic measurements. The $LaNi_{0.5}Mn_{0.5}O_{3.06}$ sample shows the highest T_C at around 260 K. This compound develops a structural phase transition at room temperature [10]. After completing the transition, the low temperature phase becomes ferromagnetic. The magnetic ordering begins at around 180 K and 150 K for $LaNi_{0.25}Mn_{0.75}O_{3.09}$ and $LaNi_{0.1}Mn_{0.9}O_{3.13}$ samples, respectively. The magnetic moment depends, for a given x, on the preparation conditions: the oxidized samples show a lower value of magnetic moment. This difference seems to increase with increasing the Mn content of the sample, *i.e.* the difference between $LaNi_{0.1}Mn_{0.9}O_{3.13}$ and $LaNi_{0.1}Mn_{0.9}O_{3.02}$ samples is higher than between $LaNi_{0.25}Mn_{0.75}O_{3.09}$ and $LaNi_{0.25}Mn_{0.75}O_{3.0}$ samples. This effect should be related with the higher oxidation degree of the first compound.

$LaNi_{0.5}Mn_{0.5}O_{3.06}$ and $LaNi_{0.1}Mn_{0.9}O_{3.13}$ develop a structural phase transition with decreasing temperature. In both cases, the ferromagnetism only appears in the low temperature phase and the rhombohedral phase is not magnetic.

The refined magnetic moments for all samples at low temperature are summarized in Table 2 and they compare quite well to the saturated magnetic moments in the case of stoichiometric samples. These moments agree with the expected value for fully polarized transition metal magnetic moments (considering Ni^{2+} and a mixture of Mn^{3+} and Mn^{4+} as ionic approximation). Oxidized samples instead, show smaller magnetic moments and the ferromagnetic ordering seems not to be achieved completely. Qualitatively, the magnetic state may be more affected for over-oxidized samples due to the presence of vacancies at the Mn/Ni sites that are strongly disruptive for the magnetic exchange.

Magnetic measurements of samples with $x \geq 0.5$ have shown magnetic anomalies below T_C (see previous section). However, no anomalies are detected in our neutron patterns (either in the magnetic moment or in the structural parameters) related to these magnetic anomalies. This result allows us to discard a reentrant transition from a ferromagnetic phase into a spin-glass phase.

Finally, this study was also devoted to the study of partial ordering of Mn and Ni atoms in the $LaNi_{0.5}Mn_{0.5}O_3$ compounds. We observed small difference [10] between the X-ray and neutron patterns of $LaNi_{0.5}Mn_{0.5}O_{3+\delta}$ samples that could be explained by considering an ordering of Mn and Ni atoms and therefore, these samples would belong to the family of the so-called double perovskites. In order

Table 3. Structural parameters (lattice parameters and fractional atomic coordinates) and reliability factors (defined as Ref. [17]) for $LaNi_{0.5}Mn_{0.5}O_{3.06}$ sample. The refined magnetic moment at 1.5 K was 0.88(16) for Ni and Mn. (*) The refined occupation gives an antisite defect of around 10%.

Temperature (K)		1.5	400
Space group		$P2_1/n$	R $\bar{3}$
a (Å)		5.5031(2)	5.5172(2)
b (Å)		5.4540(2)	-
c (Å)		7.7308(4)	13.2694(5)
β (Deg.)		89.97(1)	-
La:	x	−0.0026(8)	0
	y	0.0209(5)	0
	z	0.2516(6)	0.2497
	B (Å^2)	0.25(6)	0.70(6)
*Mn:	(x y z)	(0 1/2 0)	(0 0 0)
	B (Å^2)	0.2(1)	0.40(15)
*Ni:	(x, y, z)	(1/2 0 0)	(0 0 1/2)
	B (Å^2)	0.4 (9)	0.82(9)
O1:	x	0.0674(7)	0.5608(4)
	y	0.4932(8)	0.0122(6)
	z	0.2443(14)	0.2523(2)
	B (Å^2)	0.65(12)	1.12(6)
O2:	x	0.7375(13)	-
	y	0.2830(14)	-
	z	0.0308(17)	-
	B (Å^2)	0.6(1)	-
O3:	x	0.2829(14)	-
	y	0.7335(14)	-
	z	0.5331(17)	-
	B (Å^2)	0.7(2)	-
$\chi^2/R_{wp(\%)}$		1.7 / 8.8	1.9 / 8.9
$R_{Bragg(\%)}/R_{mag(\%)}$		4.8 / 9.9	4.6 / -

to check this point, high-resolution neutron diffractograms were collected in D1A. The patterns were measured at 1.5 and 400 K to determine the crystal structure below and above the phase transition occurring at room temperature. Table 3 summarizes the results of the refinements. The refinement of the pattern at 1.5 K in the Pbnm space group (identical to the used for the rest of the samples with $x \leq 0.5$) showed poor reliability factors. The main discrepancy concerns to the calculated intensity for the first reflection indexed as (1 0 1). We proposed that a partial ordering of Ni and Mn atoms would increase the intensity of this reflection [10] and the $LaNi_{0.5}Mn_{0.5}O_3$ sample would belong to the family of double-perovskites [24,25]. Bearing in mind this hypothesis, the pattern was successfully refined in the monoclinic $P2_1/n$ space group. This is a subgroup of the Pbnm space group and it is currently found in other double-perovskites [24] such as Ca_2FeMoO_6. Figure 8 shows the accuracy of this refinement. The monoclinic unit cell has two non-equivalent positions for the

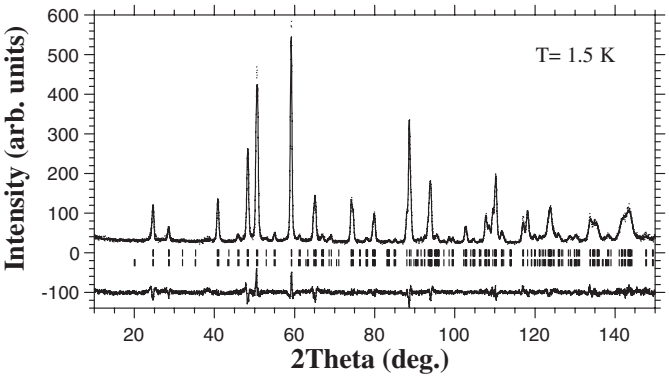

Fig. 8. Rietveld refinement of the neutron diffraction pattern at 1.5 K for $LaNi_{0.5}Mn_{0.5}O_{3.06}$. The difference between experimental (points) and theoretical (line) spectra is plotted at the bottom. The nuclear and magnetic reflections are also shown (bars).

Table 4. Distances and bond angles of the MO_6 octahedron (M= Mn and Ni) for the $LaNi_{0.5}Mn_{0.5}O_{3.06}$ sample. Multiplicity of the data and the average are also indicated in the table.

Temperature (K)	1.5	400
Space group	$P2_1/n$	R $\bar{3}$
Mn-O1 (Å)	1.925(10) × 2	1.898(3) × 6
Mn-O2(Å)	1.882(8) × 2	-
Mn-O3(Å)	1.898(8) × 2	-
$\langle$Mn-O$\rangle_{av.}$ (Å)	1.902	1.898
Ni-O1(Å)	2.012(10) × 2	2.027(3) × 6
Ni-O2(Å)	2.037(8) × 2	-
Ni-O3(Å)	2.028(8) × 2	-
$\langle$Ni-O$\rangle_{av.}$ (Å)	2.025	2.027
Ni-O1-Mn (Deg.)	158.2 × 2	162.3 × 6
Ni-O2-Mn (Deg.)	162.6 × 2	-
Ni-O3-Mn (Deg.)	161.2 × 2	-
$\langle$Ni-O-Mn$\rangle_{av.}$ (Deg.)	160.7	162.3

Ni/Mn atoms. Our refinements suggest the presence of anti-site defects, *i.e.* Ni and Mn atoms are not perfectly ordered, as reported for other double perovskites [25]. Table 4 collects the interatomic distances. One can easily distinguish two kind of MO_6 octahedra (M=Mn, Ni). The NiO_6 octahedron is bigger than MnO_6 octahedra. This result is in agreement with previous spectroscopic results [12] but the present work confirms that these octahedra are ordered in the perovskite lattice and not randomly distributed. The average Ni-O distance of 2.05 Å is usually found in oxides [26,27] with Ni^{2+} whereas the average Mn-O distance is characteristic [27] of Mn^{4+} ions. Therefore, these results confirm the oxidation state assignment of the X-ray absorption work [12].

The pattern at 400 K can be indexed in a rhombohedral unit cell but the first diffraction peak at around 24.5°,

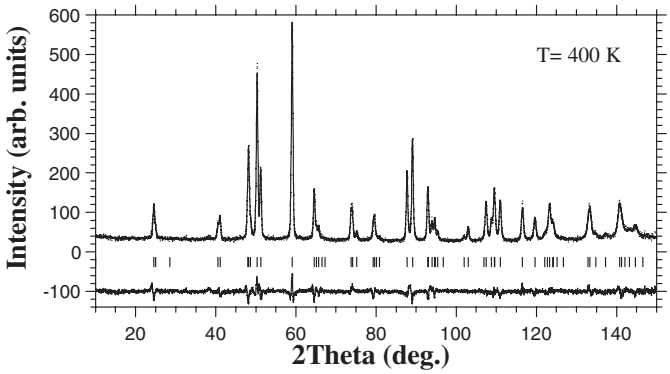

Fig. 9. Rietveld refinement of the neutron diffraction pattern at 400 K for $LaNi_{0.5}Mn_{0.5}O_{3.06}$. The difference between experimental (points) and theoretical (line) spectra is plotted at the bottom. The allowed nuclear reflections are also shown (bars).

indexed as (101)+(003), is not allowed in the R $\bar{3}$ c space group. This pattern instead, can be refined in the R $\bar{3}$ space group, a subgroup of the R $\bar{3}$ c one, as shown in the Figure 9. The results of the refinement and selected interatomic distances are shown in Tables 3 and 4 respectively. It is noteworthy that similar conclusions about antisite defects, octahedron sizes or interatomic distances can be achieved from this refinement. Actually, the structural transition at room temperature in this compound would be R $\bar{3} \rightarrow P2_1/n$ with decreasing temperature. This transition can be viewed as the equivalent to the R $\bar{3}$ c $\rightarrow$ Pbnm transition when the Mn and Ni atoms are not ordered in the lattice.

The average Mn-O and Ni-O distances are practically alike at 1.5 and 400 K (see Tab. 4). This surprising result can be ascribed to the structural phase transition developed by this sample at room temperature. Such transition is coupled to a volume expansion [10] with decreasing temperature that compensates the usual volume contraction between 400 and 1.5 K. The main structural difference between these temperatures concerns to the Mn-O-Ni bond-angle. The average Mn-O-Ni angle is smaller at 1.5 K showing that the MO_6 (M=Ni or Mn) skeleton is more distorted at this temperature though the average M-O are alike.

3.3 XMCD

Figures 10 and 11 show the normalized averaged XAS and XMCD spectra for the $LaNi_{0.5}Mn_{0.5}O_{3.06}$ sample performed at both, the Mn $L_{2,3}$ and the Ni $L_{2,3}$ edges, respectively. Each spectra has a two peak structure due to the spin-orbit splitting of the $2p$ core level into $j = 3/2$ ($2p_{3/2}$) and $j = 1/2$ ($2p_{1/2}$) sublevels. Therefore, the two main peaks represent the $2p_{3/2} \rightarrow 3d$ (L_3 edge) and $2p_{1/2} \rightarrow 3d$ (L_2 edge) transitions.

First, qualitative but important information can be drawn from the XMCD signals about the relative orientation between the Mn and Ni magnetic sublattices. A strong negative peak in the XMCD signal is observed in

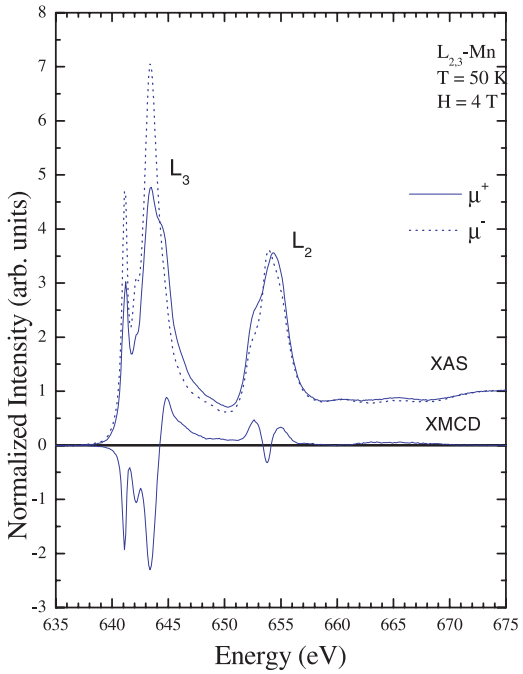

Fig. 10. Normalized Mn $L_{2,3}$ XAS spectra of $LaNi_{0.5}Mn_{0.5}O_{3.06}$ at $T = 50$ K. Solid (dotted) line refers to the spectrum taken with the direction of the applied magnetic field parallel(antiparallel) to the incident photon helicity (right). The XMCD difference spectrum resulting from the above data, after correction for the finite degree of circular polarization (83%), is also shown at the bottom.

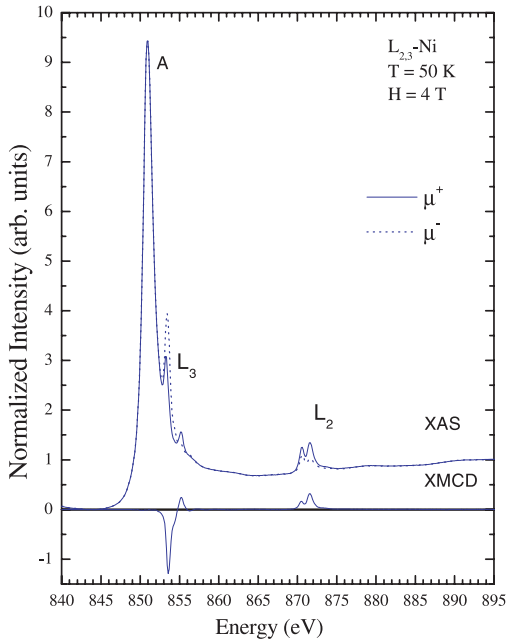

Fig. 11. Normalized Ni $L_{2,3}$ XAS spectra of $LaNi_{0.5}Mn_{0.5}O_{3.06}$ at $T = 50$ K. Solid (dotted) line refers to the spectrum taken with the direction of the applied magnetic field parallel (antiparallel) to the incident photon helicity (right). Peak A denotes the La M-edge. The XMCD difference spectrum resulting from the above data, after correction for the finite degree of circular polarization (88%), is also shown at the bottom.

both Mn and Ni L_3 regions. The direction of the magnetic moment is parallel to the direction of the applied magnetic field. Therefore, we can conclude that a parallel ordering of the net Mn and Ni magnetic moments is found for applied magnetic fields at least equal to or higher than 4 T at $T = 50$ K, in the ferromagnetic phase. This is in agreement with the previous neutron diffraction study and it allows us to discard the presence of ferrimagnetism between Mn and Ni in the $LaNi_{0.5}Mn_{0.5}O_{3.06}$ compound.

In order to extract quantitative information about the spin (m_S), orbital (m_L) and total (m_T) magnetic moment values, we apply the sum-rules in the XMCD spectra [28]. Here, we apply the sum-rules straightforwardly, assuming that the border between the $2p_{3/2}$ and $2p_{1/2}$ regions is 650 eV for the Mn L edge and 865 eV for the Ni L edge and neglecting the contribution of the magnetic dipole operator $\langle Tz \rangle$.

The orbital to spin magnetic moment ratio (m_L/m_S) is calculated to be about 0.13 for the Mn atom and 0.145 for the Ni atom. These values imply a large orbital contribution to the magnetic moment of the Mn atom ($m_{L,Mn} \approx 0.1\mu_B$) in comparison with other doped rare earth manganese oxides [29,30] whereas a value $m_{L,Ni} \approx 0.042\mu_B$ is obtained for the Ni atom (we discuss about this value later on). The estimated absolute errors are within 5–10%. This enhancement of the orbital contribution has been found when the $3d$ electrons are relatively localized and the $3d$ orbital is less or more than half-filled in it [31]. However, applicability of the sum-rules in the present case should be discussed. First, in order to apply the spin-sum-rule, the $2p_{3/2}$ and $2p_{1/2}$ regions should be well separated in the spectra. A non-zero positive XMCD signal between the Mn $2p_{3/2}$ and $2p_{1/2}$ regions is clearly shown in Figure 10 which strongly indicates that the spin-orbit splitting of the Mn core hole is not large enough to prevent the mixing of J contributions of both L_3 and L_2 edges. So, an error as large as 200% could be found in the determination of m_S, as it has been reported elsewhere [30]. This fact is not so important in the case of the Ni atom (see Fig. 11) as the spin-orbit coupling is larger and a deviation from the m_S sum-rule about 10% is assumed for this atom [32]. Secondly, an overlapping exits between the Ni L_3 edge and the La M_4 edge (peak A in Fig. 11). This overlapping does not affect the XMCD signal calculation as the La^{3+} ion is non magnetic but it is very critical for the calculation of the integrated XAS signal that is needed to determine separately the values of the orbital m_L and spin m_S magnetic moments. So, additional errors could be introduced in the estimation of m_L and m_S values for the Ni atom due to these background problems.

Anyway, we have applied the sum-rules to both Ni and Mn $L_{2,3}$ edges to establish a comparison with the magnetization and neutron diffraction results. We have obtained total magnetic moments, $m_{Ni} \approx 0.66\mu_B$ and $m_{Mn} \approx 1.76\mu_B$. These values are far below of the expected ones for a fully polarized assembly of Ni^{2+} and Mn^{4+} ions. Moreover, they do not address with the moments calculated from neutron diffraction (an average of $1.8\mu_B$) and it probably arises from a large deviation of the calculated XMCD signal as discussed above. Therefore, XMCD gives important qualitative results (it confirms the collinear ferromagnetism) but quantitative data must be taken into account carefully.

4 Discussion and conclusions

$LaMnO_3$ is an antiferromagnetic compound with ferromagnetic interactions within the (001) plane. The hole doping induces ferromagnetism as was observed in [14,33] $La_{1-x}Ca_xMnO_3$ or [15] $LaMnO_{3+\delta}$. The appearing of ferromagnetism is then coupled to the disappearing of the Jahn-Teller distortion [14]. Similar effects are found in the replacement of Mn by Ni in $LaMnO_3$ or in related samples [34]. This substitution also induces the formation of Mn^{4+} (hole doping) while Ni is +2 state. Moreover, the orthorhombic distortion arising from the tetragonal distortion of MnO_6 octahedron is strongly reduced for $LaNi_{0.1}Mn_{0.9}O_{3+\delta}$ samples. Nevertheless, this trend is reinforced in this case by the strong Ni^{2+}-O-Mn^{4+} ferromagnetic interaction that makes the substitution of Mn by Ni very effective to achieve the ferromagnetic ground state. The presence of collinear ferromagnetism has been confirmed by means of neutron diffraction and XCMD measurements. The increase of Ni content in the $LaNi_{1-x}Mn_xO_3$ series leads to an increase in the T_C but to a decrease of the average ferromagnetic moment due to the smaller magnetic moment for Ni^{2+}. Then, the Ni^{2+}-O-Mn^{4+} ferromagnetic interaction seems to be preponderant and a large ordering of Ni^{2+} and Mn^{4+} ions is found for $LaNi_{0.5}Mn_{0.5}O_{3+\delta}$ samples. T_C is almost constant but a strong reduction of the magnetization (see Fig. 3 for instance) is observed for samples with higher content of Ni. No contribution arising from ordered magnetic moments has been detected in neutron diffraction experiments. However, magnetic isotherms at 5 K show spontaneous magnetization and the χ_{ac} curves show anomalies below T_C that were ascribed to thermal freezing processes of ferromagnetic regions with different sizes [11]. The features associated to samples with $x < 0.5$ (Ni-rich region) seems to be correlated with the change in the Ni electronic configuration observed by means of the XANES spectroscopy [12]. The Ni atom is in mixed valency (2+ and 3+ states) in samples of the Ni-rich region. A possible explanation of their magnetic properties is that the Ni subband is not localized in the Ni-rich region samples as occurs for $LaNiO_3$. The ferromagnetic interactions should arise from the Mn sublattice that polarizes the surrounding Ni atoms. This would lead to ferromagnetic clusters embedded in a non-magnetic matrix, *i.e.* a glassy ferromagnet [11]. This picture is in agreement with the isothermal magnetization curves. They are composed by a spontaneous magnetization and a positive slope at high magnetic fields (magnetic saturation is not achieved). We noticed that the positive slope decreases with increasing the temperature [11] in agreement with a paramagnetic component superimposed to the ferromagnetism. Nevertheless the presence of antiferromagnetic interactions cannot be discarded.

Finally, we are going to focus on the exotic magnetic properties found in $LaNi_{1-x}Mn_xO_3$ samples with $x \geq 0.5$. These samples show ZFC-FC irreversibility in the magnetization curves and dynamical effects in the ac susceptibility measurements. It is noteworthy that there is not homovalent substitution in this system [12]. Therefore, Ni and Mn are mainly in a mixed valence state along the $LaNi_{1-x}Mn_xO_3$ series. This implies the presence of a large variety of competitive magnetic interactions (mainly: AFM superexchange Ni-O-Ni and $Mn^{\nu+}$-O-$Mn^{\nu+}$, ν being 3 or 4; FM superexchange Ni^{2+}-O-Mn^{4+}, and FM double exchange Mn^{3+}-O-Mn^{4+}) that together with the structural disorder (random distribution of Ni and Mn atoms for $x \neq 0.5$ or antisite defects for $x = 0.5$) would produce an inhomogeneous magnetic ground state. The presence of ferromagnetic and spin-glass (or cluster-glass) regions could account for the simultaneous presence of dynamical effects and long-range ferromagnetism for $x \geq 0.5$. This could be a suitable explanation for oxidized samples where the localized magnetic moments obtained from neutron patterns are below the saturated magnetic moments (see Tab. 2). However, stoichiometric samples such as $LaNi_{0.1}Mn_{0.9}O_{3.02}$ and $LaNi_{0.75}Mn_{0.25}O_{3.0}$, show similar macroscopic properties in the magnetic measurements (see Figs. 3–5) and there is not significant controversy between localized and saturated magnetic moments. This result suggests that the majority ferromagnetic phase could also be responsible of the magnetic irreversibility and dynamic effects. This is no new in ferromagnets. Recently, neutron diffraction experiments [35,36] on $La_{1-x}Sr_xCoO_3$ samples have shown long-range ferromagnetism in samples described as prototype of cluster-glass system [23,37]. This result made some authors [38] explain the dynamic and thermomagnetic irreversibility of $La_{1-x}Sr_xCoO_3$ samples in basis of the large magnetic anisotropy shown by these oxides. Some alloys [39] show a sharp rise in the χ' curve accompanied by a χ'' peak with increasing temperature. This behavior resembles the χ_{ac} curves of the $LaNi_{1-x}Mn_xO_3$ samples with $x \leq 0.5$ (see Fig. 4). These properties seem to arise from the unusual temperature dependence of the anisotropy constants [40] together with the contribution from domain-wall (DW) displacements. Dynamic effects in ferromagnets can arise from the vibration of DW within a pinning potential [40]. The source of pinning can be the local anisotropy or further effects like inclusions, structural defects or stresses. In particular, García *et al.* [41] have emphasized the importance of the magnetic disaccommodation phenomena in the magnetic properties of several intermetallic compounds. These authors proposed that DW are pinned to local defects in some ferromagnets. The defect diffusion is thermally activated so a decrease of the sample magnetization with decreasing temperature would be expected for the ferromagnetic phase. The low temperature jump in the χ' curve (see Fig. 1) can also be explained in the frame of this model as a transition from an adiabatic regime into an isothermal regime [41]. An external-alternating field excites the DW displacements. At low temperature (adiabatic regime), the defects cannot follow such displacement restraining the DW movement. The thermally activated diffusion of the local defects increases as temperature does. At high temperatures (isothermal regime), the defects can follow any DW displacement and therefore, the χ' rises with increasing temperature (see Fig. 1). Moreover, relaxation processes are also observed due to the coupling of DW and defects movements are affected by the frequency of the alternating field.

Similar effects can be thought for $LaNi_{1-x}Mn_xO_3$ oxides. There is a large amount of competitive magnetic interactions and disorder in these samples. The preponderant ferromagnetic interactions have to polarize surrounding spins to achieve the ferromagnetic ground state. This would lead to a large magnetic anisotropy and DW pinned to structural defects (mainly substitution defects or vacancies). Therefore, the magnetic properties of the system would strongly depend on the previous magnetic history of the sample, giving rise to magnetic irreversibility.

Accordingly and in basis to these results, the large amount of works [22,42–45] describing the presence of cluster-glass or spin-glass like systems in manganites should be verified by means of neutron diffraction experiments because they could actually be ferromagnets.

This work was supported by the Spanish C.I.C.Y.T. project No. MAT99-0847. The Spanish CRG beam-time on D1B (ILL) is acknowledged for neutron data and the beam- time allocation in D1A. We thank ESRF for beam-time granting. This work is dedicated to Prof. Domingo Alvarez, from the University of Zaragoza, on the occasion of his retirement.

References

1. J.M.D. Coey, M. Viret, S. Von Molnar, Adv. Phys. **48**, 167 (1999)
2. J.B. Goodenough, A. Wold, R.J. Arnott, N. Menyuk, Phys. Rev. **124**, 373 (1961)
3. N.Y. Vasanthacharya, P. Ganguly, J.B. Goodenough, C.N.R. Rao, J. Phys. C. Solid State Phys. **17**, 2745 (1984)
4. H. Fujiki, S. Nomura, J. Phys. Soc. Jpn **23**, 648 (1967)
5. A. Wold, R.J. Arnott, J. Phys. Chem. Solids **9**, 176 (1959)
6. K. Asai, H. Sekizawa, S.J. Iida, J. Phys. Soc. Jpn **47**, 1054 (1979)
7. M. Sonobe, A. Kichizo, J. Phys. Soc. Jpn **61**, 4193 (1992)
8. G. Blasse, J. Phys. Chem. Solids **26**, 1969 (1965)
9. D.D. Sarma, O. Rader, T. Kachel, A. Chainani, M. Mathew, K. Holldack, W. Gudat, W. Eberhardt, Phys. Rev. B **49**, 14238 (1994)
10. J. Blasco, M.C. Sánchez, J. Pérez-Cacho, J. García, G. Subías, J. Campo, J. Phys. Chem. Solids **63**, 781 (2002)
11. J. Blasco, J. García, M.C. Sánchez, A. Larrea, J. Campo, G. Subías, J. Phys. Cond. Matt. **13**, L729 (2001)
12. M.C. Sánchez, J. García, J. Blasco, G. Subías, J. Pérez-Cacho, Phys. Rev. B **65**, 144409 (2002)
13. J.L. García-Muñoz, J. Rodríguez-Carvajal, P. Lacorre, J.B. Torrance, Phys. Rev. B **46**, 4414 (1992)
14. E.O. Wollan, W.C. Koehler, Phys. Rev. **100**, 545 (1955)

15. C. Ritter, M.R. Ibarra, J.M. de Teresa, P.A. Algarabel, C. Marquina, J. Blasco, J. García, S. Oseroff, S.-W. Cheong, Phys. Rev. B **56**, 8902 (1997)
16. J.A.M. Van Roosmalen, E.H.P. Cordfunke, R.B. Helmholdt, J. Sol. State Chem. 110, 100 (1994)
17. J.L. Rodríguez-Carvajal, Physica B **55**, 192 (1992); J.L. Rodríguez-Carvajal, T. Roisnel, available at `http://www-llb.cea.fr/fullweb/powder.htm`
18. J. Goulon, N.B. Brookes, C. Gauthier, J. Goedkoop, C. Goulon-Ginet, M. Hagelstein, A. Rogalev, Physica B **208**, 199 (1995)
19. M. Drescher, G. Snell, U. Kleineberg, H.-J. Stock, N. Müller, U. Heinzmann, N.B. Brookes, Rev. Sci. Instrum. **68**, 1939 (1997)
20. L. Ghivelder, I. Abrego Catillo, M.A. Gusmao, J.A. Alonso, L.F. Cohen, Phys. Rev. B **60**, 12184 (1999)
21. J.A. Mydosh, *Spin glasses: an experimental introduction* (Taylor and Francis, 1993)
22. A. Maignan, C. Martin, F. Damay, B. Raveau, J. Hejmanek, Phys. Rev. B **58**, 2758 (1998)
23. S. Mukherjee, R. Ranganathan, P.S. Anilkumar, P.A. Joy, Phys. Rev. B **54**, 9267 (1996)
24. C. Ritter, M.R. Ibarra, L. Morellón, J. Blasco, J. García, J.M. de Teresa, J. Phys. Cond. Matt. **12**, 8295 (2000)
25. Y. Tomioka, T. Okuda, Y. Okimoto, R. Kumai, K.-I. Kobayashi, Y. Tokura, Phys. Rev. B **61**, 422 (2000)
26. C.A. Barret, E.B. Evans, J. Am. Cer. Soc. **47**, 533 (1964)
27. R.D. Shannon, Acta Crys., Sect. A **32**, 751 (1976)
28. B.T. Thole, P. Carra, F. Sette, G. Van der Laan, Phys. Rev. Lett. **68**, 1943 (1992); P. Carra, B.T. Thole, M. Altarelli, X. Wang, Phys. Rev. Lett. **70**, 694 (1993)
29. S. Imada, S. Suga, T. Muro, S. Ueda, R.-J. Jung, M. Kotsugi, Y. Saitoh, T. Matsushita, H. Kuwahara, H. Moritomo, Y. Tokura, Physica B **281**&**282**, 498 (2000)
30. O. Toulemonde, F. Studer, A. Barnabé, B. Raveau, J.B. Goedkoop, J. Appl. Phys. **86**, 2616 (1999)
31. S. Imada, T. Muro, T. Shishidou, S. Suga, H. Maruyama, K. Kobayashi, H. Yamazaki, T. Kanomata, Phys. Rev. B **59**, 8752 (1999)
32. Y. Teramura, A. Tanaka, T. Jo, J. Phys. Soc. Jpn **65**, 1053 (1996)
33. F. Moussa, M. Hennion, G. Biotteau, J. Rodríguez-Carvajal, L. Pinsard, A. Revcolevschi, Phys. Rev. B **60**, 12299 (1999)
34. S. Hébert, C. Martin, A. Maignan, R. Retoux, M. Hervieu, N. Nguyen, B. Raveau, Phys. Rev. B **65**, 104420 (2002)
35. V.G. Sathe, A.V. Pimpale, V. Siruguri, S.K. Paranjpe, J. Phys. Cond. Matt. **8**, 3889 (1996)
36. R. Caciuffo, D. Rinaldi, G. Barucca, J. Mira, J. Rivas, M.A. Señaris-Rodríguez, P.G. Radaelli, D. Fiorani, J.B. Goodenough, Phys. Rev. B **59**,1068 (1999)
37. For instance: M. Itoh, I. Natori, S. Kubota, K. Motoya, J. Phys. Soc. Jpn **63**, 1486 (1994); M.A. Señaris-Rodríguez, J.B. Goodenough, J. Sol. State Chem. **118**, 323 (1995)
38. P.S. Anil Kumar, P.A. Joy, S.K. Date, J. Phys. Cond. Matt. **10**, L487 (1998)
39. X.C. Kou, T.S. Zhao, R. Grössinger, F.R. de Boer, Phys. Rev. B **46**, 6225 (1992)
40. D.X. Chen, V. Skumryev, J.M.D. Coey, Phys. Rev. B **53**, 15014 (1996)
41. L.M. García, J. Bartolomé, F.J. Lázaro, C. de Francisco, J.M. Muñoz, Phys. Rev. B **54**, 15238 (1996)
42. J. Hejtmanek, Z. Jirák, M. Marysko, C. Martin, A. Maignan, M. Hervieu, B. Raveau, Phys. Rev. B **60**, 14057 (1999)
43. X.G. Li, X.J. Fan, G. Ji, W.B. Wu, K.H. Wong, C.L. Choy, H.C. Ku, J. Appl. Phys. **85**, 1663 (1999)
44. J.-W. Feng, L.P. Hwang, Appl. Phys. Lett. **75**, 1592 (1999)
45. Z.H. Wang, J.W. Cai, B.G. Shen, X. Chen, W.S. Zhan, J. Phys. Cond. Matt. **12**, 601 (2000)